In situ spectroscopic monitoring of CO_2 reduction at copper oxide electrode

Liying Wang[a], Kalyani Gupta[a], Josephine B. M. Goodall[a], Jawwad A. Darr[a] and Katherine B. Holt*[a]

DOI: 10.1039/b000000x [DO NOT ALTER/DELETE THIS TEXT]

Copper oxide modified electrodes were investigated as a function of applied electrode potential using *in situ* infrared spectroscopy and *ex situ* Raman and X-ray photoelectron spectroscopy. In deoxygenated $KHCO_3$ electrolyte bicarbonate and carbonate species were found to adsorb to the electrode during reduction and the CuO was reduced to Cu(I) or Cu(0) species. Carbonate was incorporated into the structure and the CuO starting material was not regenerated on cycling to positive potentials. In contrast, in CO_2 saturated $KHCO_3$ solution, surface adsorption of bicarbonate and carbonate was not observed and adsorption of a carbonato- species was observed with *in situ* infrared spectroscopy. This species is believed to be activated, bent CO_2. On cycling to negative potentials, larger reduction currents were observed in the presence of CO_2; however, less of the charge could be attributed to reduction of CuO. In the presence of CO_2 CuO underwent reduction to Cu_2O and potentially Cu, with no incorporation of carbonate. Under these conditions the CuO starting material could be regenerated by cycling to positive potentials.

1 Introduction

The conversion of carbon dioxide into chemical feedstock molecules and fuels is an attractive approach to addressing carbon capture and developing sustainable energy sources[1]. Electrochemical CO_2 reduction has been well-studied over many decades, and while still far from viable industrial application, improvements in practical and theoretical understanding mean significant progress is still being made towards the technological goal[2]. All of the readily available metals[3], many metal alloys[4], oxides[5] and sulphides[6] have been investigated as electrodes for CO_2 reduction. The most promising and widely studied material is copper, as it the only metal to produce hydrocarbons and appreciable quantities of $>C_1$ products during CO_2 reduction[7]. However, problems persist with poor faradaic efficiency (due to the competing H_2 evolution reaction), poor product selectivity and loss of activity over time.

The use of copper oxide electrodes in this application was first reported in 1991[8], but the field has undergone a massive resurgence over the past five years[9-18]. It has been noted by many researchers that copper electrode surface morphology and nanostructure and the presence of surface oxides plays a large role in determining product distribution and efficiency[9-18]. For this reason, the role of copper oxides and their reduction products in CO_2 reduction has been studied recently using a wide range of techniques, including X-ray diffraction[9-12], Auger[8,13,14], X-ray photoelectron spectroscopy (XPS)[10,11,13], temperature programmed desorption[15,16], X-ray absorption spectroscopy[14,15,17]. Relatedly, semiconducting copper oxides are also proposed as

promising photocatalysts for CO_2 photo-reduction, hence their performance under reducing conditions is of interest[19].

The exact nature of the active catalyst when copper oxide electrodes are used is still under question. This is because CuO undergoes reduction at the potentials employed for CO_2 reduction and hence is reduced to Cu(0). The prevailing opinion at present is that metallic Cu is the catalyst under reaction conditions, regardless of the starting material[9-12,16-18]. The most effective catalysts (in terms of overpotential, faradaic efficiency, selectivity and ability to produce higher hydrocarbons) are nanostructured copper electrodes formed from reduction of oxide-derived copper (OD-Cu)[10]. These electrodes are formed through annealing of copper in air to form thick Cu_2O films and are proposed to retain metastable Cu(0) sites at grain boundaries when electrochemically reduced[12]. It is these Cu(0) sites, rather than oxides or Cu(I) sites that provide the extraordinary activity towards CO_2 and CO reduction[10,12,16]. Other studies, employing *in situ* X-ray absorption spectroscopy to monitor the Cu K-edge of different Cu(I) and Cu(II) catalyst precursors during CO_2 reduction, have likewise suggested that only metallic copper is the catalytic species and that the oxidation state of the precursor is unimportant[17].

In contrast, a number of studies using OD-Cu electrodes for CO_2 reduction claim that Cu(I) sites and the oxygen centres of copper oxide surface structures provide CO_2 binding sites and tailored reactivity that can influence overpotential and product distribution[8,14,15]. It has been proposed that Cu_2O can promote adsorbed CO_2 activation by donating electron density[8], that Cu(I) sites within its structure promote stronger binding to CO and are present throughout the catalytic process[15] and production of methanol as a reduction product is proportional to Cu(I) content[14]. Computational density functional theory studies of Cu_2O and CuO show that copper oxide surfaces do provide alternate and feasible binding sites for CO_2, that would lead to activation of the CO_2 molecule and a different product distribution to that seen on metallic copper[20,21].

In this study we use cyclic voltammetry (CV), *ex situ* XPS and Raman spectroscopy and *in situ* IR spectroscopy to gain more insight into the interaction of CO_2 with CuO electrodes during electrochemical reduction. Although extensive catalytic studies have been carried out at OD-Cu, Cu_2O and CuO electrodes, most have focussed on product distribution analysis, along with some before and after electrode characterisation. Relatively few *in situ* measurements of the catalyst material have been reported[15,17]. Here we study the initial interaction of the CO_2 with the catalyst surface at low overpotentials during the first potential cycle, to determine how CO_2 binds to the CuO surface. Additionally, we determine how the presence of CO_2 in solution influences the reactivity of the CuO material and in particular how the oxidation state of the copper centres changes during potential cycling.

2 Experimental Materials and Procedures

2.1 CuO synthesis and characterisation

Copper (II) oxide nanoparticles were synthesised by continuous hydrothermal flow synthesis and characterised by powder X-Ray Diffraction (XRD) and Transmission

Electron Microscopy (TEM)[22]. The material was confirmed as CuO (tenorite) by XRD and the average particle diameter by both XRD and TEM is approximately 15 nm.

2.2 Experimental procedures

2.2.1 Cyclic Voltammetry (CV)

A working electrode of boron-doped diamond (BDD) modified with a layer of CuO was used, along with a counter electrode of platinum and a Ag / AgCl reference electrode. The working electrode was constructed by drop-coating CuO suspended in isopropanol onto the BDD electrode and allowing the solvent to evaporate. Aqueous electrolytes were prepared using Millipore deionised water (18 MOhm cm) and 0.5 M $KHCO_3$. Solutions were deoxygenated by bubbling through high-purity argon for 20 minutes and then maintaining a flow of argon above the electrochemical cell during measurements. Solutions were CO_2 saturated after deoxygenation with argon, by bubbling high purity CO_2 that had been through two washing stages to remove organic contaminants. All experiments were repeated three times with freshly prepared electrodes to ensure reproducibility.

2.2.2 X-ray Photoelectron Spectroscopy (XPS)

Electrodes suitable for subsequent XPS analysis were prepared using glassy carbon rods of length *ca*. 10 cm and diameter 3 mm (Sigma Aldrich). CuO was coated onto the rods by drop-coating from isopropanol. The CuO-modified rods were stored in a vacuum desiccator overnight to ensure the removal of all of the isopropanol. Electrodes were held at different potentials in the $KHCO_3$ electrolyte, or cycled (see text), removed from the solution, dried under an argon stream and stored in glass vial before XPS analysis. XPS measurements were carried out using a Thermo Scientific K-Alpha spectrometer with Al K-alpha X-rays (1486.6 eV) and a 400 µm spot size. Three random spots were analysed per rod to ensure reproducibility. XPS spectra were peak fit using CasaXPS software with a Shirley background, making use of standard XPS databases and other literature[23]. Relative composition of the surface species were calculated from peak areas and the relevant sensitivity factors.

2.2.3 Raman Spectroscopy

CuO-modifed carbon rods were prepared in an identical manner to that described above for XPS and stored in preparation for Raman analysis. A Renishaw inVia Raman Microscope with 514.5 nm laser was used, with spectra obtained from at least three random positions on the rod to ensure reproducibility. A background spectrum of the carbon rod without the CuO coating was featureless in the 100-800 cm^{-1} region shown in this study.

2.2.4. *In situ* attenuated total reflectance infrared (ATR IR) spectroscopy

An electrochemical cell was constructed above the diamond prism of the internal reflectance element of a Bruker Tensor ATR IR spectrometer. The working electrode was a BDD electrode modified with CuO, as described in section 2.2.1. The working electrode was placed directly above the prism, with an electrode–prism spacing of approximately 15 µm. The CuO coating is in contact with both the electrode and the prism, but as the evanescent wave of the incident IR penetrates at most 2 µm above the prism, only the CuO furthest from the electrode surface is probed by the IR. Different potentials were applied to the working electrode in 0.5 M $KHCO_3$ with and without CO_2, and the IR spectra measured at the different potentials relative to a

background. Experimental conditions are described further in the text.

3 Results and Discussion

3.1 Stability of CuO under potential cycling in 0.5 M $KHCO_3$ in the absence of CO_2

3.1.1. Cyclic Voltammetry of CuO-modified electrode in deoxygenated $KHCO_3$

The CV of a freshly prepared CuO-modified electrode was obtained by cycling from -0.4 V to -1.2 V, then to 0.4 V and back to -0.4 V in deoxygenated 0.5 M $KHCO_3$ solution, as shown in Fig 1. Initially currents are close to zero, indicating the presence of a passivating layer on the CuO surface, however reduction currents begin to flow at *ca*. -0.7 V (I). Reduction currents increase in magnitude negative of -1.0 V (II) and bubbles appear on the electrode surface, indicating that hydrogen evolution is taking place at this potential. No oxidation processes are noted on the reverse scan until *ca*. -0.2 V when the first of two overlapping oxidation peaks (III, IV) are observed. On cycling back to -0.4 V a reduction peak is seen at *ca*. -0.25 V (V). Previous studies[24] have assigned (I) as the reduction of Cu(II) oxide to Cu(I) oxide or Cu(0); (II) as proton reduction; (III) and (IV) as oxidation of Cu(I) or Cu(0) species to Cu(II) oxides or hydroxides and (V) as reduction of the Cu(II) products of (III) and (IV) to Cu(I) oxide. To aid with assignment of these processes Raman spectroscopy and XPS of the CuO electrodes were carried out after application of different potentials.

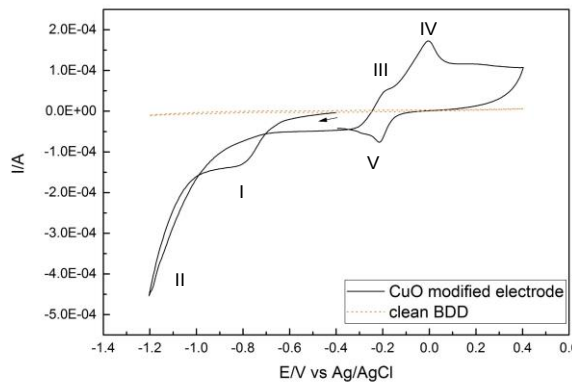

Fig. 1 CV of bare BDD (orange) and first scan of freshly CuO-modified BDD (black) electrode in Ar deoxygenated 0.5 M $KHCO_3$ electrolyte, scan rate 100 mV s^{-1}. Peak labels I – V as defined in text.

3.1.2. X-ray Photoelectron Spectroscopy of CuO electrodes after application of different potentials

CuO-coated carbon rod electrodes were held at potentials of -0.4 V, -0.8 V or -1.2 V for 15 min in 0.5 M $KHCO_3$ deoxygenated solution and their composition analysed *ex situ* using XPS. High resolution XPS Cu 2p spectra for the electrodes are shown in Fig 2. The spectrum obtained for the electrode held at -0.4 V (A) is identical to that for the electrode before potential was applied (not shown). Both unused and -0.4 V

treated electrodes show a Cu(II) $2p_{3/2}$ peak at 935.3 eV, a Cu(II) $2p_{1/2}$ peak at 955.6 eV and well-defined Cu(II) $2p_{3/2}$ and $2p_{1/2}$ satellite peaks at 944.6 eV and 963.3 eV respectively[25]. The spectrum in both cases is consistent with only CuO being present on the surface.

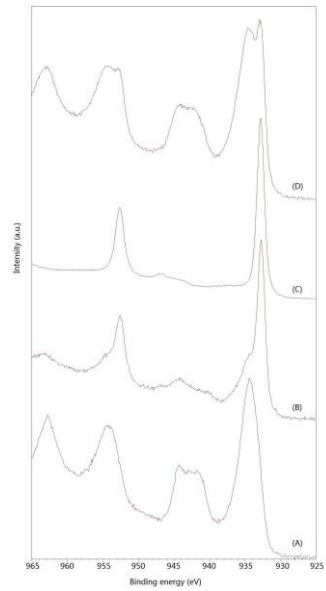

Fig. 2 High resolution Cu 2p XPS spectra for a CuO-coated carbon rod electrode after application of potential for 15 min in Ar deoxygenated 0.5 M $KHCO_3$ solution (A) -0.4 V; (B) -0.8 V; (C) -1.2 V; (D) one full cycle from 0 V to -1.2 V to 0.4 V then back to 0 V.

After treatment at -0.8 V, the spectrum (B) shows the Cu(II) $2p_{3/2}$ and $2p_{1/2}$ peaks at 934.9 and 955.1 eV, as well as additional peaks at 932.9 eV and 952.6 eV. These new peaks can be assigned to Cu(I) or Cu(0) $2p_{3/2}$ and $2p_{1/2}$ photoelectrons[23]. The peak position and full width half maximum for Cu(0) and Cu(I) species are too similar to allow us to discriminate between the two oxidation states. The areas under the Cu(II) $2p_{3/2}$ and Cu(0)/Cu(II) $2p_{3/2}$ peaks, along with the sensitivity factor for Cu, were used to determine the relative proportion of oxidised and reduced species on the surface. After treatment at -0.8 V the proportion of Cu(II) falls from 100% to 56%, indicating that nearly half of the copper within the sampling depth of the technique is reduced. This is consistent with the assignment of reduction peak I in Fig 1 to reduction of Cu(II)O. Treatment at -1.2 V (C) results in complete loss of the Cu(II) peaks, with the spectrum only showing the Cu(0)/Cu(I) peaks at 932.8 eV and 952.5 eV. As XPS is a surface sensitive technique, this indicates that the top several monolayers of CuO are completely reduced by treatment at -1.2 V, although the bulk may remain unchanged.

A CuO electrode was also subjected to a complete potential cycle from 0 V to -1.2 V to 0.4 V and back to 0 V. Inspection of Fig 1 shows the electrode should undergo the reduction processes I and II and then the oxidation processes corresponding to peaks III and IV. However, as the cycle stops at 0 V, the electrode will not undergo the

reduction process indicated by peak V. The Cu 2p spectrum after a complete cycle (D) showed a mixture of Cu oxidation states present on the surface, corresponding to 85% Cu(II) and 15% Cu(0)/Cu(I). This indicates that the reduced Cu species products formed during the negative-going sweep are not fully oxidised back to Cu(II) on scanning positive beyond peaks III and IV.

3.1.3. Raman Spectroscopy of CuO electrodes after application of different potentials

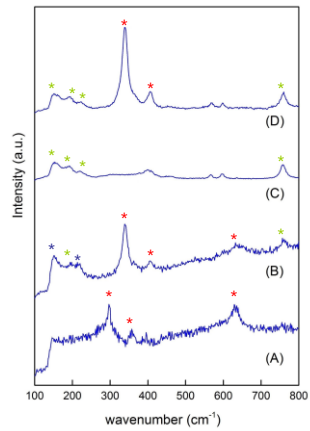

Fig. 3 Raman spectra for a CuO-coated carbon rod electrode after application of potential for 15 min in Ar deoxygenated 0.5 M $KHCO_3$ solution (A) -0.4 V; (B) -0.8 V; (C) -1.2 V; (D) one full cycle from 0 V to -1.2 V to 0.4 V then back to 0 V. Red asterisk: CuO modes; blue asterisk: Cu_2O modes; green asterisk: Cu carbonate modes.

As above, CuO-coated carbon rod electrodes were held at potentials of -0.4 V, -0.8 V or -1.2 V for 15 min in 0.5 M $KHCO_3$ deoxygenated solution and their composition analysed *ex situ* with Raman spectroscopy. As the sampling depth of Raman is greater than for XPS we expect the resulting spectra to provide information on both surface and bulk transformations. Consistent with the XPS results the CuO electrode held at -0.4 V showed identical spectral features to an unused electrode, with peaks at *ca*. 300, 350 and 630 cm^{-1} corresponding to the A_g, B^1_g and B^2_g modes of CuO respectively[26].

After treatment at -0.8 V the spectrum changes significantly, consistent with the XPS and CV data which show that close to 50% of the Cu(II) content in the surface is converted to Cu(I) or Cu(0). Raman peaks are now present at *ca*. 150, 190, 220, 340, 400, 630 and 760 cm^{-1}. Definitive assignment of all the peaks is very difficult, as some are not consistent with any previous literature assignment for copper oxide or hydroxide species. Cu_2O is relatively well characterised in literature[27] and its Raman peaks are found at *ca*. 150, 220 and 630 cm^{-1}; these are indicated by a blue asterisk on Fig 3. The peaks at 340 and 400 cm^{-1} are tentatively assigned to Cu(II)-O modes, but are shifted from the original positions of the CuO material at 300 and 350 cm^{-1}. The peak shift and increase in intensity may result from reduction of neighbouring copper centres, or a change in bonding environment of the Cu(II) centres, perhaps due to coordination with carbonate or bicarbonate. In support of this assignment, the new peaks at 220 cm^{-1} and 760 cm^{-1} have not previously been reported for copper oxide and hydroxide species; however, Raman bands are found in similar positions for

copper carbonate minerals, such as malachite[28].

At -1.2 V the peaks at 150, 190, 220, 400 and 760 cm^{-1} remain, while the bands at 340 and 630 cm^{-1} are now absent. Additionally, a new pair of bands has emerged at 570 and 600 cm^{-1} along with a broad band at 430 cm^{-1}. The loss of the peaks at 340 cm^{-1} and 630 cm^{-1} indicate a loss of Cu(II)-O modes and this is in agreement with XPS data that showed only Cu(I) or Cu(0) present after holding at -1.2 V. Although peaks consistent with Cu_2O remain at 150 and 220 cm^{-1}, the peak at 630 cm^{-1} is no longer present. As this peak is expected to be the strongest band for Cu_2O, its absence suggests that Cu_2O is also not present in the sample. Most of the remaining peaks show similar, but not identical positions to the copper carbonate minerals azurite and malachite; in particular the band at 760 cm^{-1} is at the position expected for carbonate modes, rather than Cu-O modes[28].

After a complete potential cycle (D) the Raman spectrum does not closely resemble that of the CuO before potential is applied. XPS revealed that most of the copper returns to the Cu(II) oxidation state by the end of the cycle, although about 15% remains reduced. Most of the Raman peaks assigned to copper carbonate species remain (green asterisk), but the re-emergence of the peaks at 345 and 400 cm^{-1} indicate that these peaks can be more confidently be attributed to a Cu(II) species. However, the Cu(II) species is clearly not the same as the CuO starting material.

3.1.4. Chemical and structural changes to CuO electrode under cycling

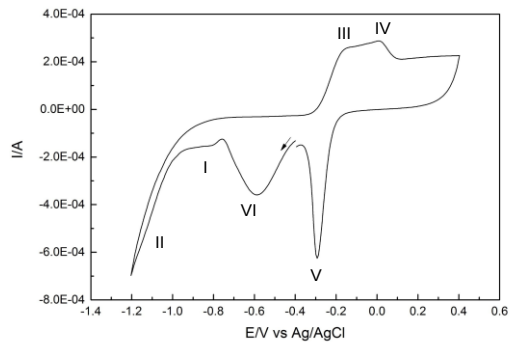

Fig. 4. Fifth CV scan of CuO-modified BDD electrode in Ar deoxygenated 0.5 M $KHCO_3$ electrolyte, scan rate 100 mV s^{-1}. Peak labels I – VI as defined in text.

From the CV, XPS and Raman data we can conclude with confidence that the reduction currents for peak I in Fig 1 result in the partial (*ca.* 50% at the surface) reduction of CuO to a Cu(I) species at -0.8 V. Some Cu_2O is present at this potential and the remaining Cu(II) has undergone some structural or coordination change, possibly in response to reduction of neighbouring groups, or due to binding of solution bicarbonate ions. Application of -1.2 V (peak II, Fig 1) results in further reduction, with loss of all Cu(II) species. No Cu_2O remains at this potential, but other Cu(I) species, for example carbonate, may be present. Reduction to Cu(0) is possible and

probable, but we are unable to distinguish between Cu(0) and Cu(I) with XPS and the Cu(0) is not Raman active. After one complete cycle most of the copper centres return to the Cu(II) oxidation state (85% at the surface), but the Raman spectrum shows that the resulting material has a different structure to the starting material (labelled as $Cu(I)/Cu(II)_{unknown}$ in further discussion).

Fig 4 shows how the CV of the CuO material evolves upon continued cycling. Peaks I – V remain but increase in magnitude with increasing scan number. Beyond scan one an additional reduction peak VI is present at *ca*. -0.6 V. This can be attributed to the reduction of $Cu(I)/Cu(II)_{unknown}$ formed during the previous cycle. A possible reaction sequence for the redox events in the first cycle is therefore:

I	$2CuO + H_2O + 2e^- \rightarrow Cu_2O + 2OH^-$
II	$Cu_2O + H_2O + 2e^- \rightarrow 2Cu + 2OH^-$ (along with H_2O reduction)
III, IV	Cu oxidation to $Cu(I)/Cu(II)_{unknown}$

Peaks V and VI are due to reduction of the $Cu(I)/Cu(II)_{unknown}$ species, which is clearly more easily reduced than the original CuO material as the reduction potentials are less negative. The current magnitude of all of the peaks increases with increased scan number indicating a thicker layer of redox-active material is generated over repeated potential cycling. The identity of $Cu(I)/Cu(II)_{unknown}$ is not clear; however, the Raman spectrum for the product is not that of $Cu(OH)_2$ (where peaks at *ca*. 300 and 490 cm^{-1} are expected)[29] or of CuO[26] or Cu_2O[27]. The material has relatively well defined and sharp Raman peaks and its spectrum resembles copper carbonate species[28], suggesting incorporation of electrolyte ions into the structure. The concluding message from this study is that at the potentials used for CO_2 reduction the catalyst material undergoes significant structural change and hence the starting material may not be the same as the active catalyst.

3.2 Stability of CuO under potential cycling in 0.5 M $KHCO_3$ in the presence of CO_2

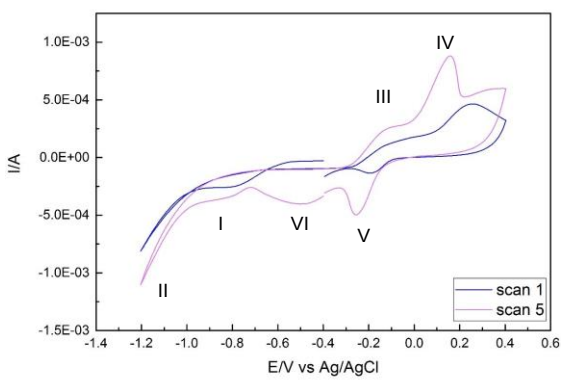

Fig. 5. First (blue) and fifth (pink) CV scan of CuO-modified BDD electrode in CO_2 saturated 0.5 M $KHCO_3$ electrolyte, scan rate 100 mV s^{-1}. Peak labels as defined in text.

The same CV, Raman and XPS investigations as described above were carried out in CO_2 saturated 0.5 M $KHCO_3$ solution. First and fifth CV scans for a CuO-modified electrode

under these conditions are shown in Fig 5. Features are broadly similar to those seen without CO_2 but in general currents are slightly higher in magnitude, reduction peaks are seen at less negative potentials, while oxidation peaks are pushed to higher positive overpotentials. Clearly the presence of CO_2 causes a change in reactivity of the CuO material, where the higher currents and decreased reduction overpotentials suggest that either the CuO material undergoes reduction more readily under these conditions, or additional reduction processes associated with the CO_2 are taking place.

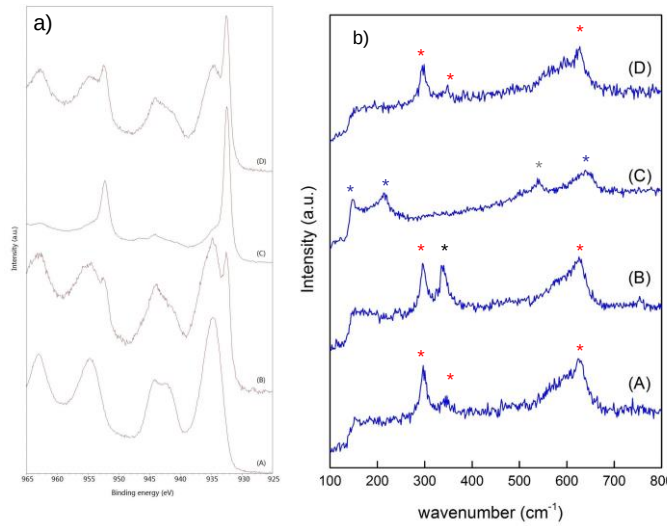

Fig. 6 (a) High resolution Cu 2p XPS spectra and (b) Raman spectra. For a CuO-coated carbon rod electrode after application of potential for 15 min in CO_2-saturated 0.5 M $KHCO_3$ solution (A) -0.4 V; (B) -0.8 V; (C) -1.2 V; (D) one full cycle from 0 V to -1.2 V to 0.4 V then back to 0 V.

The XPS data in Fig 6 a shows that the CuO actually undergoes *less* reduction in CO_2 saturated conditions, indicating that the enhanced reduction currents must be related to CO_2 reduction rather than reduction of the CuO. After holding at -0.4 V for 15 min (A) the composition of the CuO remains unchanged but after application of -0.8 V (B) the Cu 2p spectrum shows both Cu(II) and Cu(I)/Cu(0) present in a proportion of 82% and 18% respectively. In contrast, under the same conditions in Ar-saturated solution 44% of the copper was found in the reduced form. After holding at -1.2 V more of the Cu(II) is reduced, with only about 12% remaining, but in the absence of CO_2 the XPS spectrum showed no Cu(II) remaining at this potential. After completion of one cycle a mixture of Cu(II) and Cu(I)/Cu(0) species results, as observed in Ar-saturated solution. In contrast, the proportion of Cu(II) is actually lower after cycling in CO_2 saturated solution (73% in CO_2 saturated, versus 85% in Ar-saturated), showing that although reduction of the Cu(II) seems to be inhibited by the presence of CO_2, the oxidation of the resulting Cu(I)/Cu(0) species is likewise suppressed.

Raman spectroscopy further shows that the redox chemistry of CuO is substantially different when CO_2 is present in the solution. A comparison of Fig 6 b (with CO_2) and Fig 3 (without CO_2) shows clearly that the product distribution in the presence of CO_2 is far less complex. After holding at -0.4 V (A) the resulting spectrum shows only the

presence of CuO Raman peaks (red asterisk). Application of -0.8 V results in a new peak at *ca*. 340 cm^{-1} (black asterisk) while the peaks for CuO remain. The peak at 340 cm^{-1} was attributed previously to a Cu(II) species, where the copper centre is in a different bonding environment to the starting material. There are no peaks for Cu_2O present at this potential, while they were present at -0.8 V in the absence of CO_2 (Fig 3). At -1.2 V peaks at 150, 220 and 640 cm^{-1} attributed to Cu_2O emerge (blue asterisk), along with an additional peak at *ca*. 540 cm^{-1} (grey asterisk). The peaks for CuO and the unknown Cu(II) species at 340 cm^{-1} are no longer present. The peak at 540 cm^{-1} is consistent with that reported for the mixed valance Cu_4O_3 species ($Cu^{II}_2Cu^{I}_2O^{2-}_3$)[30]. After one complete cycle (D) the spectrum is identical to that of the starting material, indicating that the reactions that resulted in $Cu(I)/Cu(II)_{unknown}$ as the main product in deoxygenated solution are greatly supressed in the presence of CO_2. The Raman spectrum D appears to contradict the XPS data under the same conditions, as XPS shows that only 73% of the copper is returned to the Cu(II) oxidation state. However it may be that the remaining Cu(I)/Cu(0) species are Raman inactive, or are found in only a thin layer at the surface, where they would be readily detected by XPS but present in insufficient quantity to be detected by Raman.

In summary, the CuO catalyst undergoes less extreme changes in oxidation state and composition when the solution is saturated with CO_2. XPS shows that less of the Cu(II) undergoes reduction of Cu(II) to Cu(I) or Cu(0) and Raman spectroscopy indicates reduction to Cu_2O and Cu_4O_3, with no evidence of the carbonate formation noted in the absence of CO_2. As the CV data shows enhanced currents in the presence of CO_2, this suggests that reactions additional to the reduction of the CuO catalyst must be taking place. There are two reasons why the redox behaviour of CuO could be different in CO_2 saturated solution. The first is that the pH of the solution will decrease on addition of CO_2, as more carbonic acid is formed and dissociates:

$$CO_2 + H_2O \rightarrow HCO_3^- + H^+$$

As the redox chemistry of CuO is pH dependent, the decrease in pH may change the CuO reactivity. Secondly the $CO_{2(aq)}$ molecules may preferentially bind to the CuO surface in place of the bicarbonate electrolyte ions and undergo reduction themselves while inhibiting the reduction of the CuO. *In situ* IR experiments were therefore carried out in order to identify the surface-bound species as a function of applied potential.

3.3 In situ IR of CuO modified electrode with applied potentials

Fig 7 shows the 2000–800 cm^{-1} wavenumber range IR spectra for a CuO electrode at different potentials in the absence (a) and presence (b) of CO_2 in solution. The spectra are all recorded relative to a background of the CuO electrode equilibrated in the solution without a potential applied. The presented spectra are therefore difference spectra, with increases in absorbance indicating an increase in interfacial concentration of species absorbing at that wavenumber and decreases in absorbance indicating a loss of species absorbing at that wavenumber. The figure should be read from bottom to top with first -0.4 V being applied, then -0.8 V, then -1.2 V, returning to -0.8 V, -0.4 V then 0.4 V. The ΔAbsorbance scale for (b) is approximately 5 times that for (a), so the noise due to adventitious water vapour at 1400-1800 cm^{-1} is much more pronounced in (a).

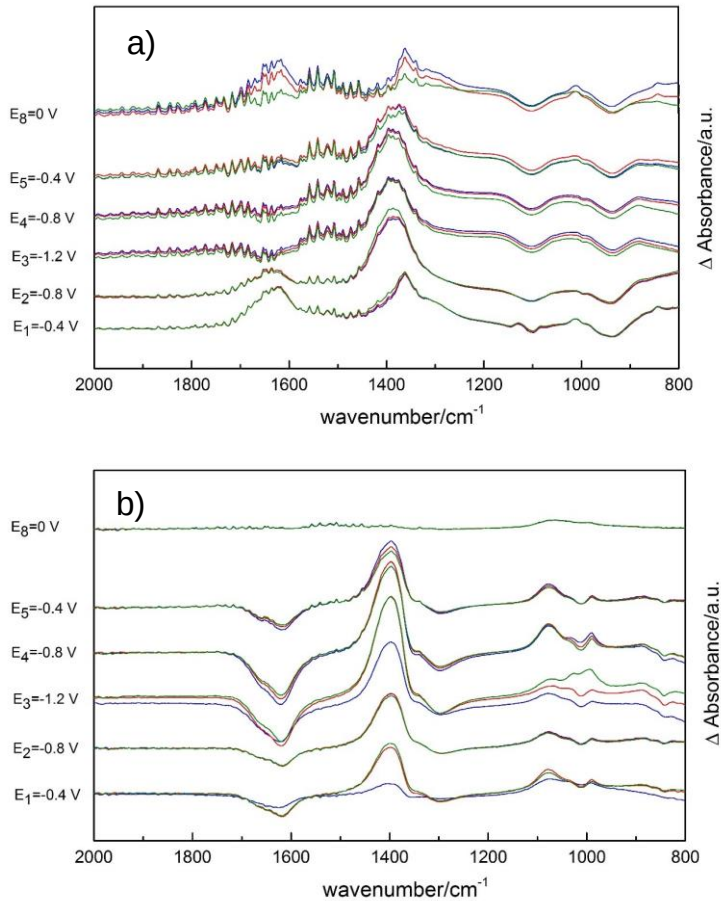

Fig. 7 ATR IR difference spectra of CuO-modified electrode under potential control (a) in argon deoxygenated 0.5 M $KHCO_3$ and (b) in CO_2 saturated 0.5 M $KHCO_3$.

In the absence of CO_2 and with application of -0.4 V (Fig 7 a), gains in absorbance are seen at 1635, 1362, 1012 and 845 cm^{-1} corresponding to bands for bicarbonate, which are slightly shifted to higher wavenumber than reported for the solution anion[30]. This increase in bicarbonate concentration on application of -0.4 V suggests that the applied potential encourages surface adsorption of the anion. Losses in absorption are seen at 950 cm^{-1} and 1120 cm^{-1}; these values do not correspond carbonate or bicarbonate vibrational modes[31], although spectral changes at similar wavenumber have been reported for CO_2 adsorption onto metal oxide surfaces and attributed to surface structure changes on adsorption[32]. On application of -0.8 V, then -1.2 V and then returning to -0.8 V the bands at 1635, 1012 and 845 cm^{-1} decrease in intensity indicating a loss of adsorbed bicarbonate from the CuO surface. The 1362 cm^{-1} bicarbonate band is replaced by a broader band centred at *ca*. 1400 cm^{-1} that indicates the asymmetric C-O stretch of carbonate[31]. When the potential is returned to -0.4 V the bicarbonate features begin to re-emerge. At 0 V the spectrum looks similar to the

initial spectrum at -0.4 V, but with an additional band at 1550 cm^{-1}, which has previously been reported for strongly coordinated bicarbonate ions on metal oxide surfaces[32].

In the presence of CO_2 the IR difference spectra are strikingly different. The intensities of the bands are much stronger and the speciation is different. At -0.4 V a decrease in intensity is seen at the position of solution bicarbonate bands at 1617, 1320, 1010 and 840 cm^{-1}. There is a concomitant increase in bands at 1400 and 1080 and 990 cm^{-1}, consistent with surface-bound carbonate species[32]. The band at *ca*. 1080 cm^{-1} is reported to be particularly characteristic of carbonato complexes[33]. This is different from the behaviour in Ar-saturated solution, where bicarbonate was the adsorbed species and losses in metal oxide surface vibrational modes were seen at 950 and 1120 cm^{-1}. In the presence of CO_2 bicarbonate is instead lost from the interfacial region to be replaced by a different adsorbed species and the same losses in metal oxide surface vibrational modes are not observed. The differences suggest that the new adsorbed species is CO_2 in a bend configuration, similar to the structure of carbonato ligands and that it binds on different surface sites to bicarbonate. As spectral features for bicarbonate are lost at the same rate, this indicates that adsorption of the CO_2 competes and is preferential. On application of -0.8, -1.2, -0.8 then -0.4 V the spectral features remain similar, although their relative intensity changes, indicating that the surface carbonato species remains bound throughout the cycle at negative potentials. At 0 V the spectrum returns to the background response obtained before application of potential, with only a band at 1080 cm^{-1} for the carbonato- species persisting.

Figure 8 shows a schematic of the possible surface species under the different conditions. Under argon, the initial adsorbing species at -0.4 V is bicarbonate, shown in Fig 8 as binding to the Cu centres via two oxygens. In pH 8 solution, hydroxide ions may be bound to the Cu centres, in which case bicarbonate would interact with the Cu-OH moieties by hydrogen-bonding. Both methods of bonding would result in spectral features for adsorbed bicarbonate and disruption to surface Cu-O-(H) vibrational modes. On application of more negative potential the bicarbonate is replaced by carbonate, possibly as a consequence of the increase in pH at the electrode interface during water reduction. Computational modelling has indicated that CO_2 binds to CuO surfaces by coordination of the central carbon atom with surface oxygen[21], as shown in Fig 8 b. Depending on the surface structure, either one or two of the oxygen atoms of CO_2 can interact with Cu centres. Either structure leads to activation of the CO_2 and a bent configuration, consistent with the observed spectral features of the carbonato species. As indicated by the spectra, the binding sites for CO_2 adsorption in this model are different from those for bicarbonate.

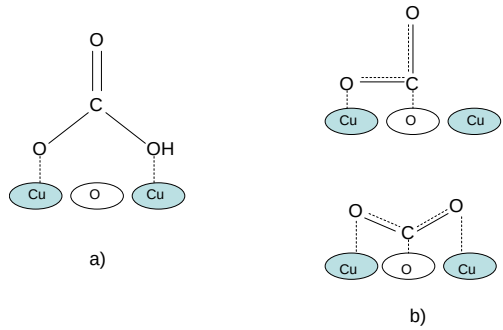

Fig. 8 Schematic of adsorbed solution species at -0.4 V in (a) argon deoxygenation 0.5 M $KHCO_3$ and (b) CO_2 saturated 0.5 M $KHCO_3$

4 Conclusion

Catalysis studies using the same CuO nano-materials as used in this work have shown that formic acid is the main product formed at the reduction potentials studied here[22]. Formic acid is also predicted as a major product by computational modelling[21]. We have shown using *in situ* IR spectroscopy that CO_2 binds to the surface of the CuO at negative applied potentials and the spectral features are consistent with a bent, activated configuration. CO_2 is found to bind to the surface at potentials where CuO has not yet undergone reduction to Cu(I) or Cu(0) species. This shows that the CuO is able to activate CO_2 without preliminary reduction taking place. XPS and Raman analysis of the catalyst material show that reduction of the Cu content is inhibited in the presence of CO_2, despite higher reduction currents being observed in the CV. This indicates that some of the charge passed may contribute to reduction of adsorbed CO_2 rather than reduction of the catalyst.

As discussed in the introduction, prevailing opinion is that copper oxide materials must first be reduced to copper to be effective CO_2 electrocatalysts[9-12,16-18]. This study does not contradict this, as it likely that the copper produced during reduction is a more active catalyst for CO_2 reduction than CuO. However, what we shown, in support of other studies[8,14,15], is that the CuO surface does allow for CO_2 activation at potentials positive of the reduction of CuO. Enhanced currents for CO_2 reduction are also observed at potentials where reduction of CuO is more likely to result in Cu_2O species rather than Cu(0), indicating the copper need not be fully reduced before allowing catalysis. We also show that the catalyst is relatively robust to cycling, especially in the presence of CO_2, where competitive carbonate complexation does not take place. However, the spectroscopic analysis carried out in the work investigated the first reduction cycle of pristine CuO and further studies are required to understand the catalytic performance under repeated cycling.

Acknowledgements

Liying Wang thanks the China Scholarship Council and UCL Industrial Doctoral

Centre for Molecular Modelling and Materials Science (EP/G036675) for funding her PhD studentship. This work was partly funded by EPSRC Grant EP/H046313.

References

[a] *Department of Chemistry, University College London, 20 Gordon St, London WC1H 0AJ, United Kingdom.*
* *Corresponding author. E-mail: k.b.holt@ucl.ac.uk*

1. For a review see: G. A. Olah, G. K. S. Prakash, A. Goeppert, *J. Am. Chem. Soc*., 2011, **133**, 12881-12898.
2. For a review see: E. E. Benson, C. P. Kubiak, A. J. Sathrum, J. M.Smieja, *Chem. Soc. Rev.*, 2009, **38**, 89-99.
3. Y. Hori, Electrochemical Reduction on Metal Electrodes.In: Vayenas et. al (eds) *Modern Aspects of Electrochemistry*, New York: Springer, 2008.
4. (i) S. Sarfraz, A. T. Garcia-Esparza, A. Jedidi, L. Cavallo, K. Takanabe, *ACS Catal*., 2016, **6**, 2842-2881. (ii) S. Y. Choi, S. K. Jeong, H. J. Kim, I.-H. Baek, K. T. Park, *ACS Sustainable Chem. Eng*., 2016, **4**, 1311-1318.
5. (i) D. D. Zhu, J. L. Liu, S. Z., Qiao, *Adv. Mater*., 2016, **28**, 3423-3452. (ii) S. Lee, J. Lee, *ChemSusChem*, 2016, **9**, 333-344.
6. (i) K. Chan, C. Tsai, H. A. Hansen, J. K. Norskov, *ChemCatChem*, 2014, **6**, 1899-1905. (ii) A. Roldan, N. Hollingsworth, A. Roffey, H. U. Islam, J. B. M. Goodall, C. R. A Catlow, J. A. Darr, W. Bras, G. Sankar, K. B. Holt, G. Hogarth, N. H. de Leeuw, *Chem. Commun.*, 2015, **51**, 7501-7504.
7. (i) K. J. P. Schouten, Y. Kwon, C. J. M. van der Ham, Z. Qin, M. T. M. Koper, *Chem. Sci*., 2011, **2**, 1902-1909. (ii) A. A. Peterson, F. Abild-Pedersen, F. Studt, J. Rossmeisl, J. K. Norskov, *Energy Environ. Sci.*, 2010, **3**, 1311-1315.
8. K. W. Frese Jr., *J. Electrochem. Soc.*, 1991, **138**, 3338 – 3344.
9. A. Dutta, M. Rahaman, N. C. Luedi, M. Mohos, P. Broekmann, *ACS Catal*., 2016, **6**, 3804-3814.
10. C.W. Li, M.W. Kanan, *J. Am. Chem. Soc.*, 2012, **134**, 7231-7234.
11. C. S. Chen, J. H. Wan, B. S. Yeo, *J. Phys. Chem. C*, 2015, **119**, 26875-26882.
12. C.W. Li, J. Ciston, M. W. Kanan, *Nature*, 2014, **508**, 504-507.
13. J. Xie, Y. Huang, H. Yu, *Front. Environ. Sci. Eng*., 2015, **9**, 861-866.
14. M. Le, M. Ren, Z. Zhang, P. T. Sprunger, R. L. Kurtz, J. C. Flake, *J. Electrochem. Soc*., 2011, **158**, E45-E49.
15. S. Lee, D. Kim, J. Lee, *Angew. Chem. Int. Ed.*, 2015, **54**, 14701-14705.
16. A. Verdaguer-Casadevall, C. W. Li, T. P. Johansson, S. B. Scott, J. T. McKeown, M. Kumar, I. E. L. Stephens, M. W. Kanan, I. Chorkendorff, *J. Am. Chem. Soc.*, 2015, **137**, 9808-9811.
17. A. Eilert, F. S. Roberts, D. Friebel, A. Nilsson, *J. Phys. Chem. Lett*., 2016, **7**, 1466-1470.
18. W. Tang, A. A. Peterson, A. S Varela, Z. P. Jovanov, L. Bech, W. J. Durand, S. Dahl, J. K. Norskov, I Chorkendorff, *Phys. Chem. Chem. Phys*., 2012, **14**, 76 – 84.
19. C. Janaky, D. Hursan, E. Endrodi, W. Chanmanee, D. Roy, D, Liu, N. R. de Taconni, B. H. Dennis, K. Rajeshwar, *ACS Energy Lett*., 2016, **1**, 332 – 338.
20. E. L. Uzanova, N. Seriani, H. Mikosch, *Phys. Chem. Chem. Phys*., 2015, **17**, 11088-11094.
21. A. K. Mishra, A. Roldan, N. H. de Leeuw, *J. Phys. Chem. C*, 2016, **120**, 2198-2214.
22. K. Gupta, M. Bersani, J. A. Darr, *J. Mater. Chem. A*, 2016, doi: 10.1039/C6TA04874A.
23. (i) National Institute of Standards and Technology XPS Database. 15 September 2012. [Accessed 10 March 2016]; Available from: ttp://srdata.nist.gov/xps/main_search_menu.aspx; (ii) X-ray Photoelectron Spectroscopy (XPS) Reference Pages. 2015. [Accessed 10 March 2016]; Available from: http://www.xpsfitting.com/

24. (i) S. Gonzalez, M. Perez, M. Barerra, A. R. Gonzalez Elipe, R. M. Souto, *J. Phys. Chem. B*, 1998, **102**, 5483-5489. (ii) D. Tromans, R. -H. Sun, *J. Electrochem. Soc.*, 1992, **139**, 1945-1951.

25. S. Poulson, P. M. Parlett, P. Stone, M. Bowker, *Surf. Interface Anal*., 1998, **24**, 811-820.

26. L. Debbichi, M. C. Marco de Lucas, J. F. Pierson, P. Kruger, *J. Phys. Chem. C*, 2012, **116**, 10232-10237.

27. A. Singhal, M. R. Pai, R. Rao, K. T. Pillai, L. Lieberwirth, A. K. Tyagi, *Eur. J. Inorg. Chem*., 2013, **2013**, 3640-3651.

28. R. L. Frost, W. N. Martens, L. Rintoul, E. Mahmutagic, J. T. Kloprogge, *J. Raman Spectrosc*., 2002, **33**, 252-259.

29. H. Y. H. Chan, C. G. Takondis, M. J. Weaver, *J. Phys. Chem. B*, 1999, **103**, 357-365.

30. C. Toparli, A. Sarfraz, A. Erbe, *Phys. Chem. Chem. Phys*., 2015, **17**, 31670-31679.

31. A. R. Davis, B. G. Oliver, *J. Solution Chem*., 1972, **1**, 329-339.

32. K. D. Dobson, A. J. McQuillan, *Langmuir*, 1997, **13**, 3392-3396.

32. K. Nakamoto, *Infrared and Raman Spectra of Inorganic and Coordination Compounds*, 3rd Ed. Wiley: New York, 1978.